^{241}Am Migration in a Sandy Aquifer Studied by Long-Term Column Experiments

ROBERT ARTINGER,*
WOLFRAM SCHUESSLER,
FRANZ SCHERBAUM,
DIETER SCHILD, AND JAE-IL KIM

Forschungszentrum Karlsruhe, Institut für Nukleare Entsorgung, P.O. Box 3640, 76021 Karlsruhe, Germany

The migration behavior of ^{241}Am(III) in a sandy aquifer was studied under near-natural conditions by long-term column experiments of more than 1 year duration. Columns with 50 cm length and 5 cm in diameter were packed with aeolian quartz sand and equilibrated with two different groundwaters having an original dissolved organic carbon concentration (DOC) of 1.1 and 7.2 mg·dm^{-3}, respectively, from the Gorleben site (Lower Saxony, Germany). In each experiment, 1 cm^3 of Am-spiked groundwater ([Am] = 0.2 to 2 μmol·dm^{-3}) was injected into the column. The flow rate of the groundwater was adjusted to 0.28 m·d^{-1}. A small colloid-borne Am fraction was found to elute together with tritiated water. After 414 and 559 days, respectively, the experiments were terminated. Whereas the nonsorbing tracer of tritiated water would have covered a distance of about 350 m in that time period, the maximum of the Am activity was detected between 32 and 40 mm column length. Applying selective dissolution analysis to the sand surface, Am was found to be preferentially bound to iron hydroxide/oxide sites. From this Am distribution, a retardation factor R of about 10^4 was determined and compared to static batch experiments. The Am breakthrough was calculated for the conditions of the column experiment.

Introduction

The mobility of radionuclides in subsurface aquifers is important in handling radioactive contaminated sites and in the long-term safety assessment of a deep geological nuclear waste disposal site. Detailed knowledge of the geochemical behavior of radionuclides is a precondition for a reliable prediction of the radionuclide mobility (*1*). Therefore, the input data for performance assessment, frequently obtained from laboratory tests, are important for application to natural conditions. Here, relevant aspects are e.g. the duration of the experiment, sample selection and heterogeneity, static or dynamic experimental approach, and the inclusion of colloids as a third phase (*2*). Depending on the experimental approach and data evaluation (e.g., equilibrium or kinetic approach), the application of laboratory data may result in strong deviating predictions of the radionuclide mobility.

Since colloid-facilitated radionuclide migration is broadly accepted (*2*−*4*), the interaction of aquatic radionuclide/colloid entities has to be taken into account in safety assessment. A mechanistic description of the relevant interaction processes, e.g. single mineral approach for metal ion sorption onto aquifer surfaces (*5*) or kinetic approach for metal ion/colloid interaction (*6*), is a precondition for the prediction of the radionuclide migration behavior. Migration experiments studying the mobility of Am(III) (*7, 8*) demonstrate that the simultaneous occurrence of a mobile and strongly retarded fraction impedes the geochemical description of Am based on thermodynamic equilibrium.

For practical reasons, batch experiments are still the most common approach to obtain data for estimating actinide mobility (e.g. refs *9*−*13*). To apply these static sorption data to natural dynamic aquifer conditions, a verification via migration experiments (e.g. ref *14*) is necessary.

The purpose of this work is to compare the Am mobility in a porous aquifer derived from batch experiments (*6, 7*) to that of dynamic column experiments with a duration of more than 1 year. Whereas the unimpeded colloid-borne Am breakthrough in column experiments and batch experiments was discussed in detail in previous studies (*6, 7*), this paper focuses more on the retarded Am fraction sorbed onto the sand surface. The column experiments were made under near-natural conditions using Gorleben groundwater/sand samples and Am(III). Destructive analysis of the sand columns was made to determine the Am mobility. Selective dissolution analysis was applied to reveal preferential mineral phases for the Am sorption onto the sand surface. Furthermore, the long-term column experiments were used to verify an own model approach (*6, 15*).

Experimental Section

Procedures and Materials. Americium migration experiments were performed using acryl glass columns of 50 cm length and 5 cm in diameter, tightly packed with Pleistocene aeolian quartz sand from the Gorleben site. Groundwater types GoHy-182 and GoHy-412, both from the Gorleben aquifer, were used. To maintain near-natural conditions, the column experiments were carried out in a glovebox with a gas atmosphere of Ar and 1% CO_2. Prior to the migration experiments, the columns were equilibrated with the groundwater over a period of 3 months. The basic parameters of equilibrated groundwater are shown in Table 1. The reducing property of equilibrated groundwater (Eh ~ -200 mV; measured by a combined redox electrode Pt4805-S7/120, Mettler Toledo Co., Switzerland) was preserved due to the contact with the sediment that facilitated redox processes.

The elemental composition of the sand surface was determined by XPS (X-ray Photoelectron Spectroscopy). Spectra were acquired by use of a XPS spectrometer (PHI Model 5600ci, Eden Prairie, MN) with monochromatic Al Kα (1486.6 eV) X-ray excitation. According to X-ray fluorescence and X-ray diffraction analysis, the uniform fine sand consists of about 85% quartz, 10 to 15% feldspar, and <5% of other minerals. Organic material is less than 0.5%. Major ion concentrations of the equilibrated groundwater and a more detailed characterization of the quartz sand can be found elsewhere (*7*).

Column experiments were performed with a Darcy velocity of 0.28 m·d^{-1}. This is somewhat higher than the highest Darcy velocities measured in the Gorleben aquifer (0.001 to 0.13 m·d^{-1}) (*16*). Tritiated water was used as a nonsorbing tracer to determine the hydraulic characteristics of the columns. In all experiments, 1 cm^3 Am-spiked groundwater ([Am] = 0.2 to 2 μmol·dm^{-3}) was injected into the columns. The Am breakthrough was measured by collecting fractions of $\sim$1 cm^3 and analyzing them using liquid

* Corresponding author phone: +49-7247-6023; fax: +49-7247-3927; e-mail: artinger@ine.fzk.de.

	groundwater/experiment number			
	GoHy-182/1	GoHy-182/2	GoHy-412/1	GoHy-412/2
column	4	6	3	3
Am concentration in spiked groundwater [μmol·dm^{-3}]	1.8	0.60	1.5	0.17
Am contact time with groundwater prior to injection t_C [d]	7	14	41	26
pH	6.3 ± 0.2	6.6 ± 0.2	6.9 ± 0.2	6.9 ± 0.2
ionic strength I [meq·dm^{-3}]	1.6 ± 0.1	nd[a]	3.7 ± 0.2	3.7 ± 0.2
DOC [mg·dm^{-3}]	6.4 ± 0.6	nd[a]	17 ± 2	17 ± 2
migration time t_M [d]	414	1.6	559	504
Darcy velocity ν_D [m·d^{-1}]	0.276 ± 0.006	0.266 ± 0.001	0.281 ± 0.014	0.281 ± 0.014
effective porosity ϵ	0.332 ± 0.002	nd[a]	0.331 ± 0.002	0.331 ± 0.002
effective pore volume V_P [dm^3]	0.331 ± 0.002	nd[a]	0.330 ± 0.002	0.330 ± 0.002
bulk density of sand ρ_b [g·cm^{-3}]	1.79 ± 0.01	1.81 ± 0.01	1.79 ± 0.01	1.79 ± 0.01
number of pore volumes passed by the flow N_{VP}	680 ± 15	2.5 ± 0.1	930 ± 50	840 ± 40
dispersion coefficient $D_{L,\,HTO}$ [m^2·s^{-1}] (derived from nonsorbing tracer HTO)	2.71·10^{-9}	nd[a]	3.06·10^{-9}	3.24·10^{-9}
dispersion coefficient $D_{L,\,Am}$ [m^2·s^{-1}] (derived from sorbed Am)	7.85·10^{-8}	nd[a]	1.01·10^{-7}	1.01·10^{-7}
mobile colloid-borne Am ($R \sim 1$) [%]	0.1 ± 0.2	0.4 ± 0.1	2.3 ± 0.8	1.6 ± 0.2
mean Am retardation R	10500 ± 1000	nd[a]	11500 ± 1000	-

[a] nd, not determined.

scintillation counting (Liquid Scintillation Analyzer B2505, Packard Instruments, Groningen, Netherlands; Cocktail Ultima Gold XR, Packard BioScience Co., Groningen, Netherlands). Am binding onto colloids prior to injection and after elution from the sand column was checked by ultrafiltration experiments using polyethersulfone membranes of 10^3 to 10^6 Dalton (Filtron Co., Microsep Microconcentrator, USA). Batch experiments with a liquid/solid ratio of 10 cm^3 groundwater to 2.5 g of sand and an initial Am concentration of 180 nmol·dm^{-3} (GoHy-182) and 43 nmol·dm^{-3} (GoHy-412), respectively, were continued up to 244 days and are described in detail in ref *7*.

Selective Dissolution Analysis. To study the Am sorption onto the sand surface, the columns were dismantled and the sand was removed in layers. The Am fraction adsorbed onto the sand was determined by γ-spectrometry. Two different selective dissolution procedures of the sand surface were applied. First, Milli-Q water, 0.1 M NaOH, and 1 M acetic acid were used as reagents in a very simplified pH-dependent approach. This procedure was aimed at distinguishing between organically bound and surface-sorbed metal ions. Whereas NaOH dissolved organic matter that had been sorbed onto the sand surface, which was visible by the deep brown color of the supernatant, acetic acid was expected to dissolve both surface-sorbed and organically bound metal ions. The extractions were carried out in series for up to 5 times in triplicate. The liquid-to-solid ratio was 15 cm^3 to 1 g wet sand (15% moisture content). Each extraction was performed in an ultrasonic bath for 1 h. For the subsequent series extractions, 10 cm^3 supernatant solution were replaced by a fresh solution in each case.

The second selective extraction procedure used was an operational three-step extraction scheme (*17*) which is sensitive to iron in different solid-phase forms. Wet sand samples (1 g, 15% moisture content) were treated with the reagents of citrate-dithionite-bicarbonate (for total Fe oxide) (*18*), NH_4-oxalate-oxalic acid (for poorly crystalline or "active" Fe oxides, pH 3 under darkness), and 1 M $MgCl_2$ (for exchangeable and salt-extractable Fe) (*19*). It has to be noted that this extraction procedure does not provide any accurate measure of a specific fraction of Fe, since none of the procedures is absolutely selective for the specific phases for which they are intended (*17*). Furthermore, the efficiency of each selective extraction step is strongly dependent on mineral size and surface area, respectively.

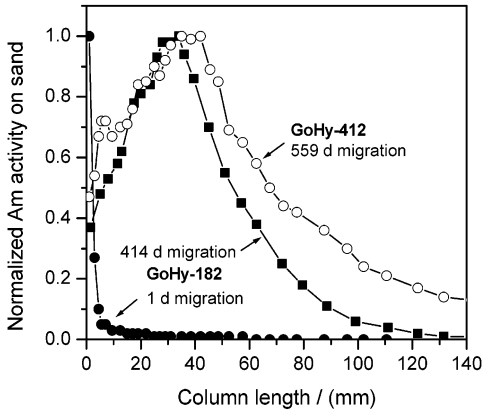

FIGURE 1. Am distribution in sand columns after the termination of the experiment. For better comparison, the Am activity concentration in the columns is normalized to the same height.

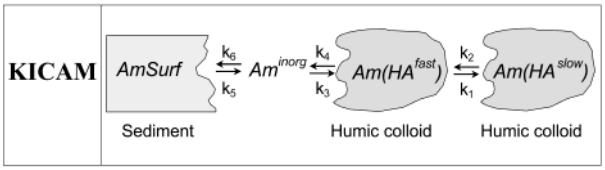

FIGURE 2. Concept of the Kinetically Controlled Availability Model (KICAM). For more details see text and ref *6*.

The solutions obtained from selective dissolution analysis were filtrated at 0.45 μm and analyzed by ICP-MS (Elan 5000, Perkin-Elmer, Rodgau, Germany) for metal ions, by ICP-AES (ARL 3580, Boush-Lomb, Lausanne, Switzerland) for Fe, and by liquid scintillation counting for Am.

Modeling

Kinetic Approach. Am(III) migration experiments (*7*) have demonstrated the need for a kinetic model. To describe these experiments, the Kinetically Controlled Availability Model (KICAM) was developed (*6*). KICAM is based on a reaction scheme (Figure 2, Table 2) with two binding modes of humic colloid-bound Am, namely, Am(HA^{fast}) and Am(HA^{slow}), suggesting different association and dissociation rates between Am and humic colloids. The rate constants were determined from batch and column experiments (*6*).

TABLE 2. Chemical Reactions and Corresponding Rate Constants Considered in KICAM (see Figure 2)

$Am(HA^{fast}) + HA \underset{k_2}{\overset{k_1}{\rightleftharpoons}} Am(HA^{slow})$	$\log(k_1 \cdot s\ mol\ dm^{-3}) = -3.2 \pm 0.2$ $\log(k_2 \cdot s) = -6.0 \pm 0.2$	(1)
$Am^{inorg} + HA \underset{k_4}{\overset{k_3}{\rightleftharpoons}} Am(HA^{fast})$	$\log(k_3 \cdot s\ mol\ dm^{-3}) = 1.5 \pm 0.5$ $\log(k_4 \cdot s) = -4.1 \pm 0.2$	(2)
$AmSurf \underset{k_6}{\overset{k_5}{\rightleftharpoons}} Am^{inorg} + Surf$	$\log(k_5 \cdot s) = -3.9 \pm 0.5$ $\log(k_6 \cdot s\ mol\ dm^{-3}) = 2.3 \pm 0.2$	(3)

Dynamic K_d Approach. Description of the colloid-borne Am transport requires a kinetic approach. To facilitate model predictions (computing time reduced by orders of magnitude), it is tempting to treat the strongly retarded Am fraction in an equilibrium way. Therefore, Am migration is split up into a nonretarded fraction (kinetic approach) and a strongly retarded fraction ("dynamic" K'_d approach). The dynamic K'_d derived from column experiments is opposed to the static K'_d as obtained from batch experiments. Dynamic distribution coefficients K'_d can be calculated from the retardation factor R determined from the Am distribution in the column using eq 1 (*20*)

$$K'_d = (R - 1)\frac{\epsilon}{\rho_b} \quad (1)$$

where ϵ is the effective porosity and ρ_b the bulk density of the sand ($g \cdot cm^{-3}$). The dimensionless retardation factor R is calculated according to eq 2

$$R = \frac{L}{x} N_{VP} \quad (2)$$

where L is the column length (50 cm), x is the covered migration length of Am in the column (in cm), and N_{VP} is the number of pore volumes passed by the flow through the column during the experiment.

Results and Discussion

Column Experiments. The long-term migration experiments using groundwater types GoHy-182 and -412 were terminated after more than 1 year. In addition, for GoHy-182, a column experiment was finished after 1 day. Results and basic parameters of the column experiments are summarized in Table 1. The mobile colloid-borne Am fraction is higher for GoHy-412 than for GoHy-182, which is attributed to the higher content of colloidal humic substances and their interaction with Am (*7*).

Activity distribution of the Am fraction retained in the column is shown in Figure 1 for all experiments. The maximum Am concentration is determined after distances of about 32 mm and 40 mm for GoHy-182 and GoHy-412, respectively. These distances reflect the mobility of surface-sorbed Am, as deduced from the experiment GoHy-182/2, showing that Am is sorbed on the very first millimeter of the sand column within 1 d. With GoHy-412, two experiments were carried out on the same column (GoHy-412/1 with 559 d migration and GoHy-412/2 with 504 d migration). Since the injected Am activity in experiment GoHy-412/1 is about nine times higher than in GoHy-412/2, the Am distribution pattern in the column is dominated by the first Am injection. From the pore volume passed by the flow through the column during the experiments (eq 2), Am retardation factors of $R = 10500 \pm 1000$ and 11500 ± 1000 are determined for GoHy-182 and GoHy-412, respectively. The error of 1000 is due to the uncertainty of the column position with the maximum Am concentration and the number of pore volumes passed by the flow through the column during the experiment (cf. eq 2).

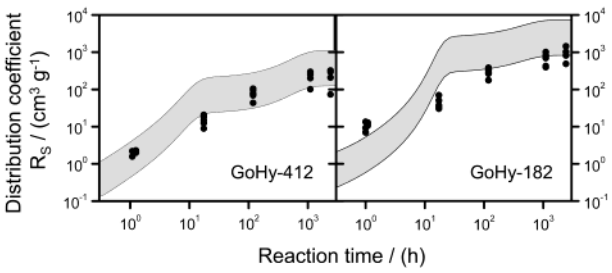

FIGURE 3. Experimental and modeling results for the temporal development of the distribution coefficient R_S in Gorleben groundwater (from ref *6*). In addition, the figure shows the R_S values with Am concentrations in the nmol·dm^{-3} range.

In accordance with eq 1, dynamic distribution coefficients of $K'_d = 1950 \pm 200\ cm^3 \cdot g^{-1}$ and $K'_d = 2150 \pm 200\ cm^3 \cdot g^{-1}$ are calculated for GoHy-182 and GoHy-412, respectively. These dynamic K'_d values are higher than the static batch values of $K'_d = 1090 \pm 90\ cm^3 \cdot g^{-1}$ for GoHy-182 and $K'_d = 505 \pm 50\ cm^3 \cdot g^{-1}$ for GoHy-412, which have been obtained after 244 d contact time under comparable conditions (*7*). In the batch experiments, Am sorption onto sand increased with increasing contact time and did not reach an equilibrium state up to 1 year (Figure 3).

The higher humic colloid concentration in GoHy-412 compared to GoHy-182 is reflected by the lower Am sorption onto the sand surface in batch experiments and the increasing mobility of the unimpeded humic colloid-borne Am in column experiments. However, no significant difference of Am retardation in the GoHy-182 and -412 column experiments could be observed. Calculations based on the concentration of surface sites and aquatic humic substances and the rate constants derived from the KICAM model (*6*) confirm this observation.

In the batch experiments, a sand-to-groundwater ratio of 2.5 g per 10 cm^3 (m/V= 0.25 $g \cdot cm^{-3}$) was used, whereas in column experiments this ratio was m/V = 5.3 $g \cdot cm^{-3}$. Taking into account the site density per g sand as determined according to Mehlich, CEC = 10^{-5} $eq \cdot g^{-1}$ (*7*), the amount of surface sites was determined to be $2.5 \cdot 10^{-3}$ and $5.3 \cdot 10^{-2}$ $eq \cdot dm^{-3}$ in the batch and column experiments, respectively. Humic colloid concentration in the groundwater GoHy-182 is $1.2 \cdot 10^{-5}$ $eq \cdot dm^{-3}$, while it reaches $8.1 \cdot 10^{-5}$ $eq \cdot dm^{-3}$ in GoHy-412 (*6*). For retarded Am migration it is important to know to what an extent an Am ion, once desorbed from the sediment, is again sorbed onto the sediment or onto humic colloids. The two reaction rates controlling these processes are $R_6 = k_6 \cdot [Surf]$ (sorption onto the sediment, see Table 2 and Figure 2) and $R_3 = k_3 \cdot [HA]$ (sorption onto humic colloids). R_6 is calculated to be 0.5 s^{-1} in batch experiments and 10.6 s^{-1} in column experiments. R_3 amounts to $3.8 \cdot 10^{-4}$ s^{-1} for GoHy-182 and $2.6 \cdot 10^{-3}$ s^{-1} for GoHy-412. In column experiments, the rate R_6 is higher by about 3 orders of magnitude than R_3. Therefore, the strongly retarded Am migration in column experiments is dominated by the sorption/desorption reaction at the groundwater/sand interface rather than by the sorption/desorption reaction of Am with the humic colloids. Hence, the different humic substance concentrations

TABLE 3. Results of Selective Dissolution Analysis for the Short-Term (1 d) and the Long-Term Migration Experiment (414 d) with GoHy-182/Gorleben Sand[a]

	extraction no.	182/1 d (0−3 mm)			182/414 d (31 mm)		
		H_2O	NaOH	HAc	H_2O	NaOH	HAc
Am (%)	1	6.0	15.5	63.0	7.3	29.0	22.4
	2	10.3	15.2	66.0	12.6	25.4	34.9
	3	12.0	17.1	74.9	14.3	24.5	45.8
	4	13.4	19.1	79.4	17.1	26.0	57.9
	5	14.3	21.5	80.5	18.5	33.8	67.5
Si ($mg \cdot dm^{-3}$)	1	nd[b]	nd[b]	nd[b]	51	680	129
	2	nd[b]	nd[b]	nd[b]	155	791	137
	3	nd[b]	nd[b]	nd[b]	175	1026	267
	4	nd[b]	nd[b]	nd[b]	219	1413	538
	5	nd[b]	nd[b]	nd[b]			
Al ($mg \cdot dm^{-3}$)	1	nd[b]	nd[b]	nd[b]	1.8	36.7	7.4
	2	nd[b]	nd[b]	nd[b]	3.3	37.8	10.5
	3	nd[b]	nd[b]	nd[b]	4.0	41.6	17.5
	4	nd[b]	nd[b]	nd[b]	5.0	46.2	28.2
	5	nd[b]	nd[b]	nd[b]			
Fe ($mg \cdot dm^{-3}$)	1	1.5	2.9	5.5	1.8	5.8	4.9
	2	2.9	2.6	7.3	4.2	4.9	6.0
	3	3.5	2.9	8.6	4.5	4.9	7.3
	4	4.2	3.2	10.1	5.1	5.3	8.4
	5	4.6	3.3	11.0			
Mn ($ng \cdot dm^{-3}$)	1	13.5	21.9	171.9	24.5	46.6	202.3
	2	25.6	19.3	173.8	36.8	37.7	200.6
	3	32.4	21.8	176.2	46.2	37.7	206.7
	4	40.0	23.6	183.3	50.1	42.6	214.2
	5	46.4	24.4	186.4			
Nd ($ng \cdot dm^{-3}$)	1	0.4	1.0	3.4	0.5	1.5	1.2
	2	0.9	1.0	4.8	1.0	1.2	2.4
	3	1.1	1.2	5.5	1.1	1.1	2.5
	4	1.4	1.1	6.7	1.4	1.5	3.4
	5	1.6	1.1	7.2			
		$MgCl_2$	oxalate	dithionite	$MgCl_2$	oxalate	dithionite
Am (%)		3.8	78	102	4.8	74.9	98.2
Fe ($mg \cdot dm^{-3}$)		nd[b]	3.0	3.8	nd[b]	4.6	6.3

[a] In case of series extraction, the extraction behavior of Am (extractable vs total sorbed Am) and accompanying elements ($mg \cdot dm^{-3}$ in extracting solution) is given by the integral dissolution. [b] nd, not determined.

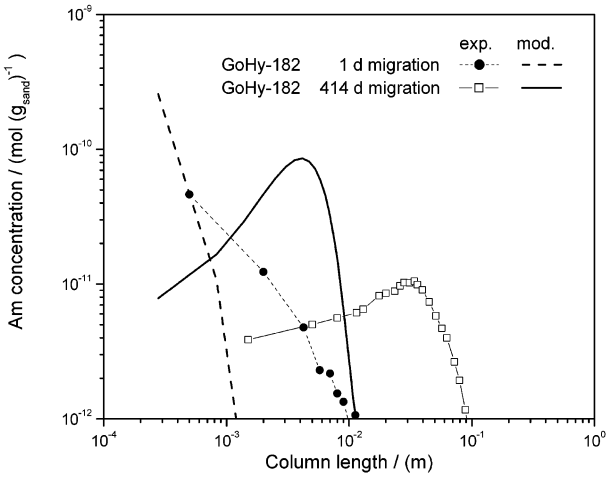

FIGURE 4. Comparison of experimental data obtained and values calculated for the Am distribution in the sand columns 4 and 6.

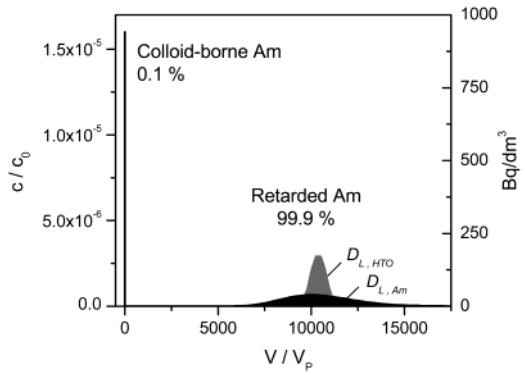

FIGURE 5. Am breakthrough curve for GoHy-182/Gorleben sand. Whereas the colloid-borne Am breakthrough is measured directly, the retarded Am fraction is calculated on the basis of the Am distribution in the column (see text). For calculation, dispersion coefficients derived from the nonsorbing tracer breakthrough (HTO) and the Am distribution in the column are used.

have less impact on the Am retardation behavior in the GoHy-182 and -412 experiments under the conditions prevailing. Comparing R_6 and R_3 in batch experiments, the association reaction onto the humic colloids becomes more important and a more pronounced effect of the humic colloid concentration is expected, as was found in the experiments (Figure 3).

The distribution of Am in the columns 4 and 6 (groundwater GoHy-182) was calculated using the K1D code (*15*) and KICAM with the parameter set given in Table 2 (as determined in ref *6*). The calculated column distributions considerably deviate from the experimental data by almost a factor of 10 in peak arrival (Figure 4). This deviation probably is due to the very simplistic treatment of the Am sand surface interaction implemented in KICAM. A similar discrepancy (about a factor of 10) is found in the description of the batch data by KICAM for GoHy-182 (Figure 3). However, the principle trend and the shape of the breakthrough curve is reproduced by the model. To enable a more accurate prediction of retarded Am migration in a porous aquifer rich

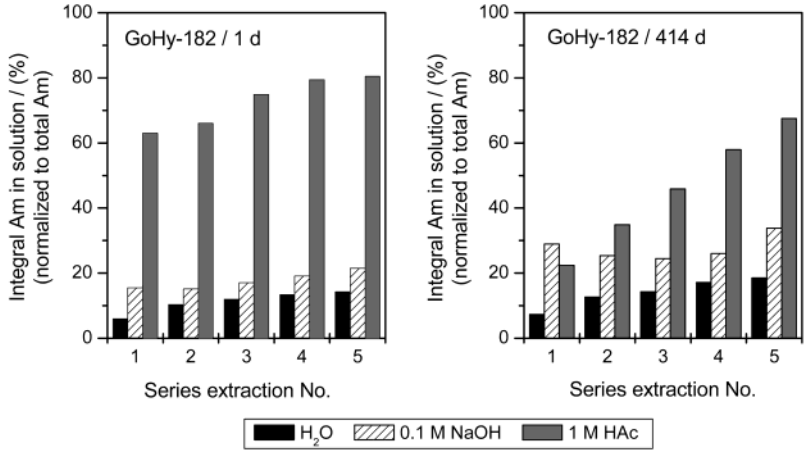

FIGURE 6. Am series extraction of Gorleben sand used in column experiments. The extracted Am is shown as an integral fraction normalized to the total Am.

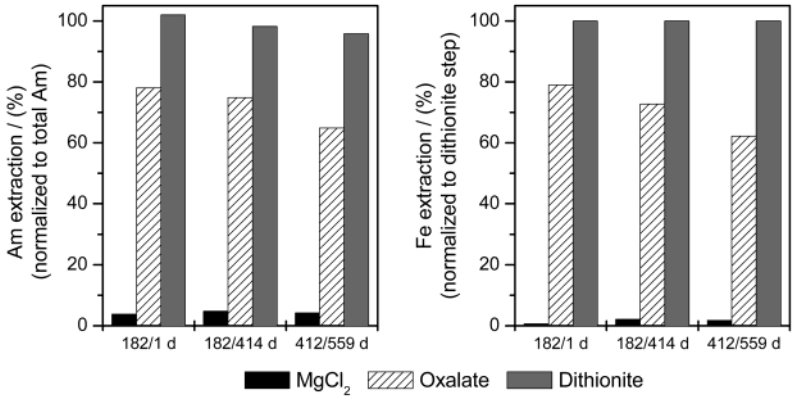

FIGURE 7. Am (left) and Fe (right) extraction of Gorleben sand used in column experiments by an iron-selective dissolution. Whereas the extracted Am concentration is given as the percentage of the total Am sorbed onto the sand, the Fe concentration is referred to the concentration extracted by the citrate-dithionite-bicarbonate step (total Fe oxide).

in humic substances, use of a dynamic K'_d still is the most appropriate approach, as will be shown below.

Combining the unimpeded colloid-borne Am breakthrough and the dynamic K'_d of the surface-sorbed Am, a complete breakthrough curve can be created for the 414 d migration experiment GoHy-182/1. For this, the breakthrough of the retarded Am was calculated according to ref *20* using the advection-dispersion eq 3 taking into account the retardation factor R of Am

$$C(x,t) = C_i + 0.5\cdot(C_0 - C_i)\cdot\left(1 - erf\left(\frac{x - \frac{v}{R}t}{\sqrt{4\frac{D_L}{R}t}}\right)\right) \quad (3)$$

where C_0 is the Am concentration in the spiked groundwater (mol·dm^{-3}) injected, $C_i = 0$, because the column initially is Am-free, x is the migration length, v is the pore water flow velocity ($v = v_D\cdot\epsilon^{-1}$) (m·s^{-1}), t is the migration time (s), and D_L is the dispersion coefficient (m^2·s^{-1}). To our knowledge, the resulting breakthrough curve of Am (Figure 5) is the first breakthrough curve for an actinide ion consisting of a clearly defined unimpeded colloid-borne and a retarded surface-sorbed Am fraction. The most remarkable result is the short in time, but drastically higher Am concentration in groundwater for the unimpeded colloid-borne fraction compared to the retarded fraction, although the colloid-borne Am fraction amounts to up to 0.1% only. Calculations for the surface-sorbed Am were performed for dispersion coefficients derived from the breakthrough of the nonsorbing tracer HTO ($D_{L,HTO} = 2.71\cdot10^{-9}$ m^2·s^{-1}) and the distribution of the sorbed Am in the column itself ($D_{L,Am} = 7.85\cdot10^{-8}$ m^2·s^{-1}), respectively. A diffusion term is not included in D_L for the prevalent pore water flow velocity of about 300 m·a^{-1}. Reasons for the differences in dispersion might be kinetic effects of the Am interaction with the sand surface. Also, a dependency of the distribution coefficient on the Am concentration may not be excluded. In this case, it may be more appropriate to apply a numerical solution to model the Am migration (e.g. mixing cells in series with defined boundary conditions) rather than to use the simple advection-dispersion eq 3. However, this requires a more advanced process description of the Am interaction with the stationary phase as it is currently available in the K1D/KICAM tool and illustrated above.

Selective Dissolution Analysis. Selective dissolution analysis was applied to obtain further information on the Am sorption onto the sand surface. Applying the reagents H_2O, 0.1 M NaOH, and 1 M acetic acid (HAc) as extractants, we analyzed different sand samples of the columns for Am and accompanying elements during the series extraction. The results of the series extraction are exemplarily summarized in Table 3 for GoHy-182 and illustrated in Figure 6. When applying sodium hydroxide as extraction reagent, up to 30% of the total amount of Am sorbed was extracted, thus indicating that Am is not preferentially bound to organics on the sand surface. Using HAc, Am was extracted up to 80%. The rate of Am extraction was significantly faster for the 1 d migration than for the 414 d migration. This indicates that Am is first sorbed onto the outermost sand surface which is easily accessible for acid extraction and then incorporated

TABLE 4. Elemental Composition of the Sand Surface as Obtained Using XPS Compared to the Bulk Composition Determined by X-ray Fluorescence Analysis

	sand surface (XPS) (at. %)	sand bulk (X-ray)	
		(at. %)	(g per kg dry solid)
Si	12.8 ± 1.3	31.8 ± 0.4	440 ± 5
Al	7.4 ± 0.8	1.1 ± 0.3	15.0 ± 4.0
Fe	2.6 ± 0.2	0.12 ± 0.03	3.4 ± 0.8
Na	1.2 ± 0.1	0.28 ± 0.03	3.2 ± 0.4
Mg	0.55 ± 0.1	0.05 ± 0.03	0.5 ± 0.1
O	55.7 ± 0.8	66.1 ± 0.2	521 ± 2

in deeper surface layers with an increasing residence time in the column.

The analysis of the Am-accompanying elements during series extraction revealed Fe as the main element with a positive correlation, indicating a possible preferential binding to Fe oxide/hydroxide phases. The positive correlation of Am and Fe applies to an extraction behavior dependent on the different reagents and pH, respectively, as well as to the extraction kinetics. From literature, such a strong affinity of Am for iron oxides (*10*, *21*) is known. On the other hand, no clear correlation was observed for the main elements Si and Al. The characterization of the sand surface by XPS confirmed the presence of Fe and, in addition, revealed an Fe enrichment on the surface compared to the bulk composition as determined by RFA (Table 4). Whereas the bulk analysis resulted in 0.1 at. % Fe, XPS surface analysis of single grains resulted in 2.6 ± 0.2 at. % Fe. Besides Fe, the lanthanide Nd is positively correlated with the Am extraction behavior. This has been expected because of the similar chemical properties of Am and Nd and again confirms the reproducibility of the extraction procedure.

To corroborate preferential Am binding to Fe oxide/hydroxide phases, a second operational three-step extraction scheme was employed. The results for the column experiments with GoHy-182 and -412 are shown in Figure 7. Using the citrate-dithionite-bicarbonate method for extraction of "total" Fe (amorphous and crystalline Fe), Am was dissolved almost quantitatively from the sand surface. Using oxalate for poorly crystalline or "active" Fe oxides, 65 to 80% of Am were extractable. The so-called exchangeable Am only is a minor fraction of about 5%, as was determined by $MgCl_2$ extraction. This is in agreement with the results of the simple water extraction. The common chemical fate of Am and Fe is also illustrated in Figure 7, showing the Am/Fe extraction pattern normalized to the citrate-dithionite-bicarbonate step.

It is important to note that the applied extraction procedures cannot give a clear proof of the dominant Am interaction with Fe oxide/hydroxide surfaces (not to mention the preferred Fe solid-phase form). Nevertheless, the results of the selective dissolution analysis of sand samples from the column experiments reveal some strong hints of the Am retardation being controlled by Fe oxide/hydroxide phases on the sand surface. Precipitation and solid-solution reactions that cause an entrapment into deeper layers, as is indicated by the extraction kinetics, may also be taken into consideration.

Acknowledgments

The authors gratefully acknowledge the technical assistance rendered by Mrs. Schlieker, Mrs. Walschburger, and Mr. Fuss. The authors would also like to thank Mr. Schäfer for his contribution to the iron-selective extraction of sediment samples and Mr. Geckeis for his contribution to the chemical analysis of the selective extraction procedures.

Literature Cited

(1) Guillaumont, R. *Radiochim. Acta* **1994**, *66/67*, 231−242.
(2) Honeyman, B. D. *Nature* **1999**, *397*, 23−24.
(3) Kersting, A. B.; Efurd, D. W.; Finnegan, D. L.; Rokop, D. J.; Smith, D. K.; Thompson, J. L. *Nature* **1999**, *397*, 56−59.
(4) Kim, J. I. *Mater. Res. Soc. Bull.* **1994**, *19*, 47−53.
(5) Waite, T. D.; Davis, J. A.; Fenton, B. R.; Payne, T. E. *Radiochim. Acta* **2000**, *88*, 687−693.
(6) Schuessler, W.; Artinger, R.; Kienzler, B.; Kim, J. I. *Environ. Sci. Technol.* **2000**, *34*, 2608−2611.
(7) Artinger, R.; Kienzler, B.; Schuessler, W.; Kim, J. I. *J. Contam. Hydrol.* **1998**, *35*, 261−275.
(8) Dierckx, A.; Put, M.; De Cannière, P.; Wang, L.; Maes, N.; Aertsens, M.; Maes, A.; Vancluysen, J.; Verdickt, W.; Gielen, R.; Christiaens, M.; Warwick, P.; Hall, A.; van der Lee, J. *Transport of radionuclides due to complexation with organic matter in clay formations* (*Trancom-Clay*); European Commission; EUR 19135; 2000.
(9) Dozol, M.; Hagemann, R. *Pure Appl. Chem.* **1993**, *65*, 1081−1102.
(10) Ticknor, K. V.; Vilks, P.; Vandergraaf, T. T. *Appl. Geochem.* **1996**, *11*, 555−565.
(11) Meier, H.; Zimmerhackl, E.; Zeitler, G.; Menge, P. *Radiochim. Acta* **1994**, *66/67*, 277−284.
(12) Tanaka, T.; Senoo, M. *Mater. Res. Soc. Symp. Proc* **1995**, *353*, 1013−1020.
(13) Torstenfelt, B.; Rundberg, R. S.; Mitchell, A. J. *Radiochim. Acta* **1988**, *44/45*, 111−117.
(14) Vandergraaf, T. T.; Drew, D. J.; Masuda, S. *J. Contam. Hydrol.* **1996**, *21*, 153−164.
(15) Schüßler, W.; Artinger, R.; Kim, J. I.; Bryan, N. D.; Griffin, D. *J. Contam. Hydrol.* **2001**, *47*, 311−322.
(16) BGR. *Übertägige geowissenschaftliche Erkundung des Standortes Gorleben*; Bundesanstalt für Geowissenschaften und Rohstoffe; 108880; 1991.
(17) Loeppert, R. H.; Inskeep, W. P. *Chapter 23. Iron*; Soil Science Society of America, American Society of Agronomy: Madison, WI, 1996.
(18) Mehra, O. P.; Jackson, M. L. *Clays Clay Miner.* **1960**, *7*, 317−327.
(19) Schwertmann, U. *Z. Pflanzenernaehr. Düng. Bodenkund.* **1964**, *105*, 194−202.
(20) Appelo, C. A. J.; Postma, D. *Geochemistry, groundwater and pollution*, 3rd ed.; Balkema: Rotterdam, 1996.
(21) Lu, N.; Kung, K. S.; Mason, C. F. V.; Triay, I. R.; Cotter, C. R.; Pappas, A. J.; Pappas, M. E. G. *Environ. Sci. Technol.* **1998**, *32*, 370−374.